International Journal of Thermophysics (2020) 41:139
https://doi.org/10.1007/s10765-020-02709-5

Density of Liquid Iridium and Rhenium from Melting up to the Critical Point

M. Leitner[1] · **G. Pottlacher**[1]

Received: 18 June 2020 / Accepted: 7 July 2020 / Published online: 31 July 2020

Abstract
The density as a function of temperature was determined for liquid iridium (Ir) and rhenium (Re) by means of shadow imaging in ohmic pulse-heating experiments. In addition to regular experiments at 0.23 MPa, high-pressure experiments at static pressures between 0.18 GPa to 0.30 GPa were performed to increase the metals' boiling point and thus determine density data at temperatures far exceeding the boiling temperature at atmospheric pressure. By this means, the experimentally accessible liquid range could be extended by roughly 2000 K (Ir) and 6000 K (Re) compared to data reported in the literature. In a second step, the experimental data were used to estimate critical temperature, critical density, and the complete phase diagram in the density–temperature plane. A comprehensive comparison with literature data was conducted.

Keywords Critical point data · High pressure · Iridium · Liquid metals · Liquid-phase density · Phase diagram · Pulse-heating · Rhenium

1 Introduction

The density of liquid metals and alloys is of high interest in many fields of engineering and science. Density data are for instance used to calculate mass balance in refining operations or to deduce further thermophysical properties such as thermal conductivity and diffusivity, viscosity, or surface tension. Most importantly, density data are used in various simulations that model physical processes, such as thermal natural convection in furnaces and ladles or casting and solidification [1–3]. Many of these physical models show a relatively strong sensitivity on density input

✉ G. Pottlacher
pottlacher@tugraz.at

M. Leitner
matthias.leitner@tugraz.at

[1] Institute of Experimental Physics, Graz University of Technology, NAWI Graz, Petersgasse 16, Graz 8010, Austria

data compared to other thermophysical properties applied during the modeling process [4]. Therefore, precise data on density as a function of temperature in the liquid phase are needed. While the density is mostly well known throughout the solid phase, the situation is different in the liquid phase, where data are scarce for some transition metals. Furthermore, data reported in the literature are often inconsistent with each other, do not reach far into the liquid phase, or exhibit large uncertainties. These observations motivate a complementary revisit on the liquid-phase density of selected metals, such as iridium and rhenium. While typical pulse-heating experiments performed previously at Graz University of Technology addressed a multitude of thermophysical properties simultaneously, Schmon suggested to conduct exclusive density measurements in combination with other measures in order to improve density data quality [5]. Metals and alloys already addressed in this exclusive approach are Ni and Cu [6], $Cu_{86}Mn_{12}Ni_2$ [7], $TiAl_6V_4$ [5], Al [8], Ta [9], Nb and W [10], $Cr_{18}Ni_{12}Mo_2$ (NIST SRM 316L) [11] and now Ir and Re. For the latter six examples, the experimental setup was recently further improved in terms of better signal-to-noise ratio, faster image acquisition rate, and reduced camera exposure times [12].

The experimentally obtained liquid-phase density as a function of temperature can be used to estimate the metal's full phase diagram, i.e., how the density of the liquid and gaseous metal changes with temperature up to the critical point. This unique point in the phase diagram, where liquid and vapor saturation lines meet and all properties of the coexisting phases are equal to each other, is not only of scientific interest but is also important in high temperature technologies, such as in aerospace and in power engineering. In the latter, critical point data are applied in potential fission-reactor accident calculations and are used for future fusion reactor designs [13]. Besides, phase diagrams and critical points are of immediate interest in astro- and planetary physics, where modelers rely on data describing the response of metals at extreme temperatures and pressures [14]. The approach used in this work follows a recent publication of Schröer and Pottlacher, where the measured liquid-phase density is extrapolated according to simplified non-linear models yielding estimates for the phase diagram and the critical point [15]. This extrapolative approach is limited by the metal's boiling point, which poses a natural upper temperature limit for the input data. Therefore, efforts were taken to increase the boiling point by performing high-pressure pulse-heating experiments in addition to those performed at almost ambient pressure.[1] Opposed to the boiling temperature, the melting temperature of metals shows only a very weak pressure dependence. Thus, the liquid phase is greatly extended and provides a richer basis for the extrapolative estimation of the investigated metal's phase diagram and critical point.

[1] The latter will be referred to as low-pressure experiments in the following.

2 Experimental Method

The method of ohmic pulse-heating was applied to resistively heat Ir and Re sample wires with 0.5 mm in diameter and an approximate length of 40 mm from room temperature (295 K) up to their boiling point. At this point, the sample explodes due to the large discontinuous jump in volume and gives the method its popular name *exploding wire technique*. Energy for the heating process is provided by a 540 µF capacitor bank that can be charged to a voltage between 3 kV to 10 kV. Once the experiment is started, a current that can peak in more than 10 kA runs through the wire sample and rapidly heats it with heating rates on the order of $10^8\,\mathrm{K}\cdot\mathrm{s}^{-1}$. These high heating rates lead to a very short experimental duration of typically 35 µs to 80 µs, depending on the specimen and experimental parameters used, and offer several advantages: First, the method can be considered quasi-containerless, i.e., chemical reactions with the surrounding atmosphere may be neglected. Second, the wire sample remains unaffected by gravity which allows the experimenter to perform measurements in the liquid phase as the wire specimen does not collapse upon melting. Third, high heating rates additionally suppress an axial expansion of the wire specimen. As the experiment can be considered quasi-static, which implies an increased radial expansion to compensate for the absent axial expansion, it is sufficient to monitor the radial expansion throughout the experiment to derive the sample's volume expansion as a function of time. For this purpose, a specialized CCD-camera system was used (PCO imaging, controller unit by Theta System and Graz Univ. of Technol.) in combination with a high-power photo flash (Multiblitz X10AC/DC, $1000\,\mathrm{W}\cdot\mathrm{s}$) that allows an image acquisition rate of 4×10^5 fps, i.e., approximately one shadow image every 2.5 µs at an exposure time of 300 ns. Each shadow image has a resolution of (8×384) pixel. For further details on the expansion measurement setup, the reader is referred to [5, 12].

In addition to the measurement of thermal radial expansion, the sample's surface radiance is monitored throughout the experiment by means of pyrometry to derive the sample temperature as a function of time. The pyrometer used operates at a central wavelength of 649.7 nm (FWHM = 37.2 nm, sampling rate: 10 MHz). Neutral density filters are applied to cover a broad temperature range.

To physically extend the accessible temperature range by raising the sample's boiling point, low-pressure pulse-heating experiments at 0.23 MPa were complemented by high-pressure pulse-heating experiments at 0.18 GPa to 0.30 GPa. While the low-pressure experiments were conducted in nitrogen (Alphagaz 1 N_2, 99.999 %), distilled water was used in high-pressure experiments to build up pressure. A detailed description of the setups may be found in [12, 16]. Note, that the high static pressure has negligible impact on density measurement due to the very small compressibility of these metals of $\kappa_{T,\mathrm{Ir}} = 0.0082\,\mathrm{GPa}^{-1}$ and $\kappa_{T,\mathrm{Re}} = 0.0092\,\mathrm{GPa}^{-1}$ [17]. Therefore, density data obtained on different isobars in the kbar-regime are typically indistinguishable for most metals, compare also [13].

Table 1 Specifications of investigated wire specimens

	Purity/wt%	Diameter/mm	Condition	Supplier	Catalog no.	ID no.
Ir	99.9	0.5	Temper annealed	Advent	IR524809	Gi2147
Re	99.99	0.5	Temper annealed	Advent	RE545909	Gi4101

Table 2 Utilized literature data for temperature deduction and density conversion of the metals iridium and rhenium

Metal	$\varepsilon(684.5\ \mathrm{nm}, T_\mathrm{r})/1$	Validity range/K	T_m/K	$\rho_0/\mathrm{kg}\cdot\mathrm{m}^{-3}$
Ir	$0.3293 + 7.988\times10^{-6}\,T_\mathrm{r}/\mathrm{K}$ [18]	$2365 < T_\mathrm{r} < 3650$	2719 [19]	22 562 [20]
Re	$0.3130 - 8.5186\times10^{-6}\,T_\mathrm{r}/\mathrm{K}$ [21]	$2870 < T_\mathrm{r} < 4100$	3458 [22]	21 020 [23]

Normal spectral emissivity $\varepsilon(\lambda, T_\mathrm{r})$ at a wavelength of 684.5 nm as a function of radiance temperature T_r, true melting temperature T_m and room-temperature density ρ_0

All sample wires were treated with abrasive paper (grade 1200) and cleaned with acetone prior to the experiment. Reported data for Ir consist of nine independent experiments (six low-pressure and three high-pressure experiments), those of Re are composed of seven independent experiments (four low-pressure and three high-pressure experiments). Table 1 lists the specifications of the wire samples used.

3 Data Evaluation

Thermal expansion and surface radiance of the sample are both measured as a function of time. These quantities are evaluated as described in the following by using literature data for melting temperature, normal spectral emissivity, and room-temperature density, as specified in Table 2. From the resulting density as a function of temperature, a phase diagram and the critical point can be estimated. In-depth details on the data evaluation as well as an exemplary thermogramme and expansion sequence have been published recently [9, 12]. Therefore, the authors focus only on the most important details here.

3.1 Temperature

The temperature evaluation is based on Planck's law of radiation. In a first step, the radiance temperature at melting is calculated using the known melting temperature T_m and the normal spectral emissivity at melting ε_m, compare Table 2. This temperature is then assigned to the melting-plateau that is visible in the radiance-over-time development to derive a radiance temperature $T_\mathrm{r}(t)$ as a function of time t. The radiance temperature as a function of time is then used in conjunction with normal spectral emissivity $\varepsilon(\lambda, T_\mathrm{r})$ to calculate the true temperature $T(t)$ as a function of time t

according to Eq. 1, where λ is the mean effective wavelength of the pyrometer and c_2 is the second radiation constant,

$$T(t) = \frac{c_2}{\lambda \cdot \ln\left\{\varepsilon(\lambda, T_r) \cdot \left[\exp\left(\frac{c_2}{\lambda \cdot T_r(t)}\right) - 1\right] + 1\right\}}. \quad (1)$$

Note that applying a gray-body assumption, the slight shift of approximately 30 nm between pyrometer wavelength and the wavelength at which emissivity data are reported can be neglected. The reported normal spectral emissivity was further assumed to continue linearly above the stated temperature validity range. A more detailed description of the evaluation procedure was already published elsewhere [9, 12].

3.2 Density

The acquired shadow images of the thermally expanding vertical wire are processed by summation over the pixel lines. The resulting intensity values as a function of x-pixel position show a clear cup-shaped intensity profile, compare [9]. The FWHM of each of these profiles at specific instants in time t is used as diameters $d(T)$ at the corresponding temperatures T. These values are related to the room-temperature pixel-diameter d_0 that is captured before the pulse-heating start. Due to the suppression of axial wire expansion, and the quasi-static behavior of the method, the wire's volume expansion $(V(T)/V_0)$ may be simply described by the square of the radial expansion $(d(T)/d_0)^2$ [24, 25]. The conversion to density as a function of temperature $\rho(T)$ is achieved in relating this measured thermal radial expansion to the room-temperature density ρ_0,

$$\rho(T) = \rho_0 \cdot \left(\frac{d_0}{d(T)}\right)^2. \quad (2)$$

3.3 Critical Point and Phase Diagram Data

On the basis of experimentally obtained liquid-phase density data, the material's phase diagram in the temperature–density plane and its critical temperature and density are estimated. The algorithm used follows a recent publication by Schröer and Pottlacher [15]. For a complementary detailed step-by-step description, the reader is also referred to [12]. The core of the algorithm is a non-linear extrapolation of the experimentally obtained density–temperature behavior according to simplified models. The approach uses a heuristic crossover from Ising to mean-field behavior to estimate the critical temperature T_c and uses a combination of the rule of rectilinear diameter and the theory of complete scaling to estimate the critical density ρ_c. In particular, the arithmetic mean between the critical temperature estimates obtained from an Ising-like extrapolation (exponent $\beta = 1/3$) and from a mean-field-like

Table 3 Fit coefficients a and b for the liquid-phase density ρ as a function of temperature T in the form $\rho(T) = a - b \cdot T$

	a	b	$U_c(\rho) \cdot \rho^{-1}$	Temperature range
	$10^3\ \mathrm{kg \cdot m^{-3}}$	$\mathrm{kg \cdot m^{-3} \cdot K^{-1}}$	1	K
Ir	22.96 ± 0.20	1.17 ± 0.05	0.012 to 0.049	$2719 \leq T \leq 9160$
Re	21.0 ± 0.4	0.77 ± 0.05	0.021 to 0.065	$3485 \leq T \leq 11\,800$

The fit was calculated combining the obtained high-pressure and low-pressure data sets. The temperature range of applicability is given. The relative combined expanded density uncertainty $U_c(\rho) \cdot \rho^{-1}$ at a fixed temperature T is given from the beginning of the liquid phase (first value) up to the highest temperature measured (second value). All uncertainties are reported at a 95 % confidence level ($k = 2$)

extrapolation (exponent $\beta = 1/2$) serves as a reasonable estimate for T_c. Similarly, the arithmetic mean between critical density obtained assuming a linear phase diagram diameter variation (exponent $\gamma = 1$) and a non-linear diameter variation (exponent $\gamma = 2/3$) is reported as reasonable estimate for ρ_c. With T_c and ρ_c fixed, a simplified phase diagram is then constructed according to Eq. 3,

$$\rho_{\pm}(T) = \rho_{\mathrm{diam}} \pm b \cdot (T_c - T)^{1/3}\left(1 + b_2 \cdot (T_c - T)^{2/3}\right), \tag{3}$$

where $\rho_+(T)$ and $\rho_-(T)$ describe the saturated liquid and saturated vapor line, i.e., how liquid and vapor density change as a function of temperature up to the critical point. $\rho_{\mathrm{diam}}(T)$ describes the phase diagram diameter which is the average between saturated liquid and saturated vapor density, modeled by

$$\rho_{\mathrm{diam}}(T) = \rho_c\left(1 + a \cdot (T_c - T) + c \cdot (T_c - T)^{2/3}\right). \tag{4}$$

The phase diagram coefficients a, c, b and b_2 in Eqs. 3 and 4 are obtained during fitting this phase diagram model to the experimentally obtained density data.

4 Results and Discussion

4.1 Density

Iridium Density as a function of temperature of iridium is depicted in Fig. 1. The plotted linear regression was calculated combining high-pressure and low-pressure data sets and considering their individual T and ρ uncertainties. The corresponding fit coefficients are given in Table 3. Experimental data points are tabulated in Table 4.

The obtained density as a function of temperature exhibits a very good consistence with the literature at the end of the solid phase and at the beginning of the liquid phase, where a density of $\rho(T_{m,l}) = (19.78 \pm 0.24) \times 10^3\ \mathrm{kg \cdot m^{-3}}$ ensues from the combined linear regression. This value is in excellent agreement to all three literature sources, residing within the stated $k = 2$ uncertainty interval.

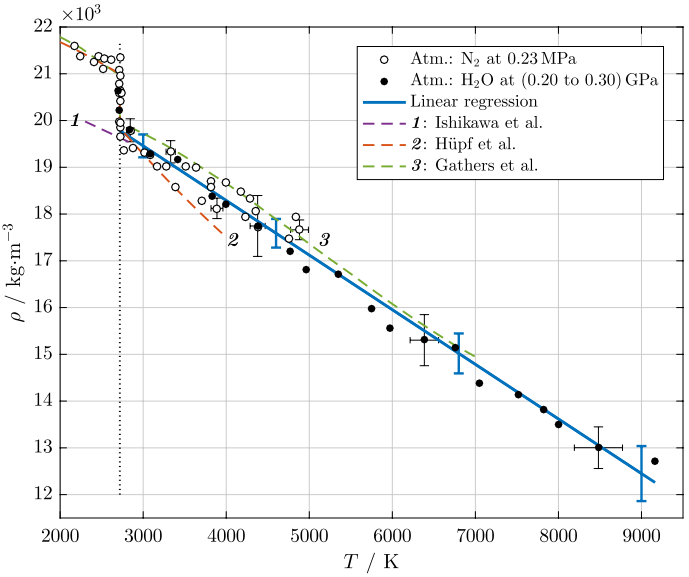

Fig. 1 Density ρ as a function of temperature T of iridium. The dotted vertical line marks the melting temperature. Symbols and solid line: This work's experimental data and corresponding linear regression of the combined data set. All uncertainties are given at a 95 % confidence level ($k = 2$). Dashed lines represent data reported in the literature: Ishikawa et al. [26], Hüpf et al. [27], Gathers et al. [28]

Ishikawa et al. [26] report a density value at the liquidus point that is 0.75 % lower than this work's value. The decrease in density with temperature reported by Ishikawa et al. is slightly less pronounced than in this work but in very good agreement. The authors used a levitation method, undercooling a liquid metal droplet in vacuum. Owing to the undercooling, density data at temperatures below the melting temperature are to be understood as an extension of the liquid phase.

Previous data reported by our group[2] (Hüpf et al. [27]) are in excellent agreement at the beginning of the liquid phase, being 0.35 % higher than this work's data. However, the extraordinary strong decrease of liquid-phase density with temperature could not be reproduced. Data reported by Hüpf et al. were acquired with the low-pressure setup in argon atmosphere.

Gathers et al. [28] report a value at the beginning of the liquid phase that is 0.92 % higher than this work's value. The consistence in both solid and liquid phase is remarkable and resides within or very close to the 95 % uncertainty interval throughout the whole reported data range. These data were acquired with a pulse-heating technique at a pressure of 0.3 GPa in inert gas atmosphere.

Rhenium Density as a function of temperature of rhenium is depicted in Fig. 2. The linear regression shown was calculated combining low-pressure and

[2] Published thermal expansion data were converted into density data with the room-temperature density stated in Table 2.

Table 4 Iridium: Experimentally obtained data points of density ρ as a function of temperature T obtained in low-pressure (atm.: N_2 at 0.23 MPa) and high-pressure pulse-heating experiments (atm.: H_2O at 0.20 GPa to 0.30 GPa)

LP-data				HP-data	
T/K	ρ/kg · m^{-3}	T/K	ρ/kg · m^{-3}	T/K	ρ/kg · m^{-3}
2173	21 600	3009	19 321	2695	20 632
2237	21 383	3084	19 256	2714	20 229
2412	21 247	3164	19 030	2836	19 809
2462	21 367	3276	19 021	3080	19 280
2514	21 109	3331	19 331	3409	19 167
2534	21 336	3383	18 586	3828	18 391
2613	21 290	3511	19 021	3993	18 221
2708	21 092	3633	18 987	4378	17 745
2715	19 965	3701	18 294	4775	17 204
2716	20 595	3810	18 700	4965	16 823
2718	20 793	3820	18 582	5355	16 710
2720	19 844	3889	18 122	5755	15 985
2723	19 946	4003	18 667	5972	15 567
2724	20 642	4178	18 487	6386	15 303
2726	21 340	4230	17 930	6756	15 134
2729	19 664	4285	18 333	7051	14 393
2731	20 412	4350	18 070	7521	14 137
2735	20 586	4388	17 716	7829	13 830
2768	19 354	4756	17 470	7997	13 502
2844	19 791	4843	17 942	8482	13 003
2884	19 400	4882	17 663	9163	12 717

Density values were derived applying a room-temperature density of $\rho_0 = 22\,562\,\mathrm{kg \cdot m^{-3}}$ [20]. Combined expanded uncertainty between the beginning of the liquid phase ($T_m = 2719\,\mathrm{K}$) up to the highest temperatures measured: $U_{c,LP}(T)/T = 0.016$ to 0.022, $U_{c,LP}(\rho)/\rho = 0.013$ and $U_{c,HP}(T)/T = 0.018$ to 0.037, $U_{c,HP}(\rho)/\rho = 0.038$ to 0.034. Uncertainties stated at a 95 % confidence level ($k = 2$)

high-pressure data sets and considering their individual T and ρ uncertainties. The corresponding fit coefficients are given in Table 3. Experimental data points are tabulated in Table 5.

Only a few valid data points in the liquid phase could be obtained by means of low-pressure pulse-heating because of evolving inhomogeneities in sample diameter. These inhomogeneities, leading to an apparent increased expansion, render an evaluation impossible. However, this problem could be suppressed by increasing the static pressure acting on the sample's surface in high-pressure experiments.

At the beginning of the liquid phase, the combined data evaluation yields a density of $\rho(T_{m,l}) = (18.3 \pm 0.4) \times 10^3\ \mathrm{kg \cdot m^{-3}}$.

This value is in excellent agreement with that reported by Paradis et al. [29], being only 0.34 % higher than this work's value. The concordance of the slope of liquid density as a function of temperature with this work's data is in extraordinary

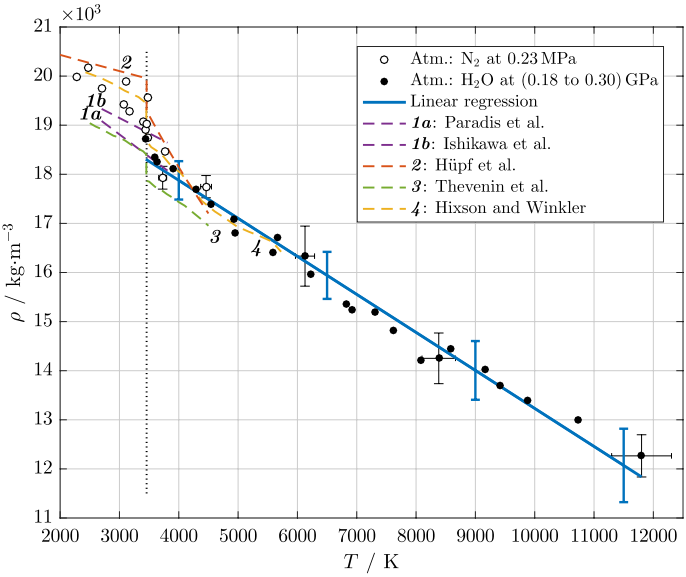

Fig. 2 Density ρ as a function of temperature T of rhenium. The dotted vertical line marks the melting temperature. Symbols and solid line: This work's experimental data and corresponding linear regression of the combined data set. All uncertainties are given at a 95 % confidence level ($k = 2$). Dashed lines represent data reported in the literature: Paradis et al. [29], Ishikawa et al. [26], Hüpf et al. [30], Thévenin et al. [31], Hixson and Winkler [32]

agreement. However, recently published data by the same working group (Ishikawa et al. [26]) are 3.1 % higher than our data at the liquidus point. Data reported by these authors were acquired by investigating a levitated liquid metal droplet at a pressure of 10^{-5} Pa in a super-cooled liquid state. Data reported below the melting temperature are thus an extension of the liquid-phase density to lower temperatures.

Data published previously by our group[3] (Hüpf et al. [30]) show a deviation in density already at the end of the solid phase. At the beginning of the liquid phase, the Hüpf value is 5.2 % higher than this work's data imply, thus outside the uncertainty boundaries. Especially the decrease in density with temperature reported in these previous data is questionably strong and inconsistent with this work's data as well as with other data reported in the literature. The data were acquired with the low-pressure setup in argon atmosphere. Given the arising problems observed when using this very same setup suggests that evolving inhomogeneities in sample diameter may be the reason for the strong density gradient reported previously by Hüpf et al.

Density data reported by Thévenin et al. [31] are inconsistent with our data at the end of the solid phase. There, the density is as low as other authors report at the beginning of the liquid phase. In the liquid phase, the slope of density as

[3] Published thermal expansion data were converted into density data with the room-temperature density stated in Table 2.

Table 5 *Rhenium* Experimentally obtained data points of density ρ as a function of temperature T obtained in low-pressure (atm.: N_2 at 0.23 MPa) and high-pressure pulse-heating experiments (atm.: H_2O at 0.20 GPa to 0.30 GPa)

LP-data		HP-data	
T/K	ρ/kg · m^{-3}	T/K	ρ/kg · m^{-3}
2284	19 985	3444	18 727
2478	20 176	3595	18 354
2698	19 744	3630	18 256
3065	19 432	3899	18 104
3117	19 879	4299	17 690
3164	19 274	4552	17 379
3401	19 080	4935	17 097
3449	18 916	4947	16 803
3468	19 026	5584	16 413
3473	18 748	5656	16 710
3477	19 558	6128	16 333
3728	17 931	6234	15 957
3773	18 471	6828	15 361
4460	17 748	6915	15 251
		7308	15 186
		7616	14 822
		8079	14 212
		8382	14 252
		8580	14 443
		9173	14 031
		9409	13 695
		9887	13 405
		10 738	13 004
		11 801	12 265

Density values were derived applying a room-temperature density of $\rho_0 = 21\,020\,\mathrm{kg \cdot m^{-3}}$ [23]. Combined expanded uncertainty between the beginning of the liquid phase ($T_m = 3458\,\mathrm{K}$) up to the highest temperatures measured: $U_{c,LP}(T)/T = 0.018$ to 0.021, $U_{c,LP}(\rho)/\rho = 0.013$ and $U_{c,HP}(T)/T = 0.020$ to 0.043, $U_{c,HP}(\rho)/\rho = 0.039$ to 0.036. Uncertainties stated at a 95 % confidence level ($k = 2$)

a function of temperature is highly consistent with this work's data and with most of the literature data. The value at the beginning of the liquid phase is 2.6 % lower than this work's value and thus just outside the 95 % confidence interval. These data were acquired with a pulse-heating setup at a pressure of 0.12 GPa in an argon atmosphere.

Density data reported by Hixson and Winkler [32] are in very good agreement both at the end of the solid and at the beginning of the liquid phase. At the beginning of the liquid phase, the reported value is 1.9 % higher than this

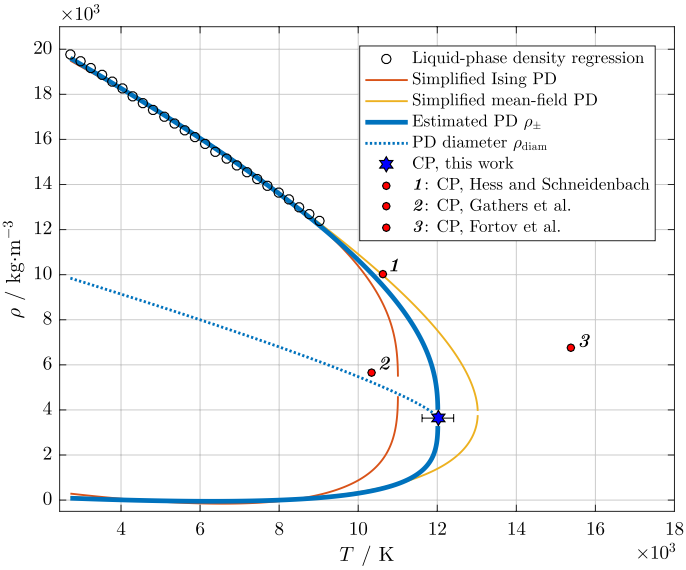

Fig. 3 Density ρ as a function of temperature T of iridium up to the critical point (CP). Open circles represent data points generated from the density regression. Thin solid lines show the estimated phase diagram (PD) according to a simplified Ising and mean-field behavior. The best estimate for the phase diagram $\rho_{\pm}$ is indicated by a thick solid line, terminating in the critical point (star). The corresponding phase diagram diameter ρ_{diam} is plotted as dotted line. Critical points reported in the literature are indicated by red dots: Hess and Schneidenbach [33], Gathers et al. [28], Fortov et al. [34]

Table 6 Estimated phase diagram parameters of the investigated high-melting metals according to Eqs. 3 and 4

	ρ_c	T_c	a	c	b	b_2
	$\mathrm{kg \cdot m^{-3}}$	K	$10^{-5}\ \mathrm{K^{-1}}$	$10^{-3}\ \mathrm{K^{-2/3}}$	$\mathrm{kg \cdot m^{-3} \cdot K^{-1/3}}$	$10^{-4}\ \mathrm{K^{-2/3}}$
Ir	3636	12 015	8.28	2.13	379	5.11
Re	3472	16 248	5.66	1.66	319	3.91

Temperature range of validity from melting temperature T_m up to the critical temperature T_c of the respective metal. a, c, b and b_2 are the obtained fitting coefficients, ρ_c is the critical density

work's value. Hixson et al. used a high-pressure pulse-heating system operating at 0.2 GPa in argon atmosphere.

4.2 Critical Point and Phase Diagram Data

Summarized phase diagram data are tabulated in Table 6.

Iridium Figure 3 depicts the estimated phase diagram of iridium and its corresponding critical point. For the critical temperature T_c and the critical density ρ_c one obtains

$$T_c = (12.0 \pm 0.4) \times 10^3\ \mathrm{K}$$
$$\rho_c = (3.64 \pm 0.15) \times 10^3\ \mathrm{kg \cdot m^{-3}}.$$

When available in the literature, (T_c, ρ_c)-pairs were plotted along with this work's data in Fig. 3. It can be observed that the obtained critical density is lower than those reported in the literature, while the critical temperature resides at an intermediate position compared to the three literature sources considered.

The value reported by Hess and Schneidenbach [33], using the Likalter relation together with a vapor pressure curve, resides at a density of $\rho_c = 10.0 \times 10^3\ \mathrm{kg \cdot m^{-3}}$ which is very close to the value observed at the highest temperatures experimentally accessed. The reported value thus appears to be rather high for the critical density. However, the critical temperature $T_c = 10\,636\ \mathrm{K}$ is in good concordance with this work's prediction.

Data reported by Gathers et al. [28] using the soft sphere van der Waals model ($\rho_c = 5.6369 \times 10^3\ \mathrm{kg \cdot m^{-3}}$, $T_c = 10\,335\ \mathrm{K}$) show a satisfactory agreement with this work's critical point, although the data appear to show higher consistency with the simplified Ising phase diagram, also plotted in Fig. 3.

The critical density reported by Fortov et al. [34], $\rho_c = 6.77 \times 10^3\ \mathrm{kg \cdot m^{-3}}$, resides at a value that is incompatible with this work's experimentally obtained liquid-phase density. Even when extrapolating the data linearly, Fortov's critical point can not be reached. The reported critical temperature of $T_c = 15\,380\ \mathrm{K}$ appears rather high as well (Grosse method).

Further critical temperatures reported in the literature range between values as low as $T_c = 9723\ \mathrm{K}$ (Hess and Schneidenbach [33], Guldberg rule) to values as high as $T_c = (17\,760 \pm 790)\ \mathrm{K}$ (Lang [35], Kopp-Lang rule). Very good consistence is also achieved with a recently reported value by Blairs and Abbasi [36], $T_c = 11\,498\ \mathrm{K}$ (Guldberg rule) and with a prediction reported by Hess and Schneidenbach [33], $T_c = 12\,009\ \mathrm{K}$ (Goldstein scaling proposal).

A critical pressure of $p_c = 0.95\,013\ \mathrm{GPa}$ [28] up to $p_c = 1.55\ \mathrm{GPa}$ [33] is reported in the literature.

The influence of temperature range accessed in density measurements on the estimated critical point was investigated for iridium. The extrapolation algorithm was repeated for density fits ranging from the melting temperature to the highest temperature reached in low-pressure experiments ($T_{max} \approx 5000\ \mathrm{K}$) and from the melting point to the highest temperature reached in high-pressure experiments ($T_{max} \approx 9000\ \mathrm{K}$). The fit equation used for the analysis was kept constant applying the coefficients derived from the combined data evaluation (Table 3). In the considered temperature range, the estimated critical temperature increases by $\Delta T_c / \Delta T_{max} \approx 0.37\ \mathrm{K \cdot K^{-1}}$ while the critical density decreases by $\Delta \rho_c / \Delta T_{max} \approx 0.18\ \mathrm{kg \cdot m^{-3} \cdot K^{-1}}$ with increasing T_{max}. Over the whole considered temperature range, the critical temperature thus increases by 15 %, the critical density decreases by 18 %. Therefore, the algorithm used generally provides a lower limit for the estimated critical temperature, and an upper limit for the estimated critical density.

Rhenium Fig. 4 shows the critical point and estimated phase diagram of rhenium. For the critical temperature T_c and the critical density ρ_c one obtains by extrapolation

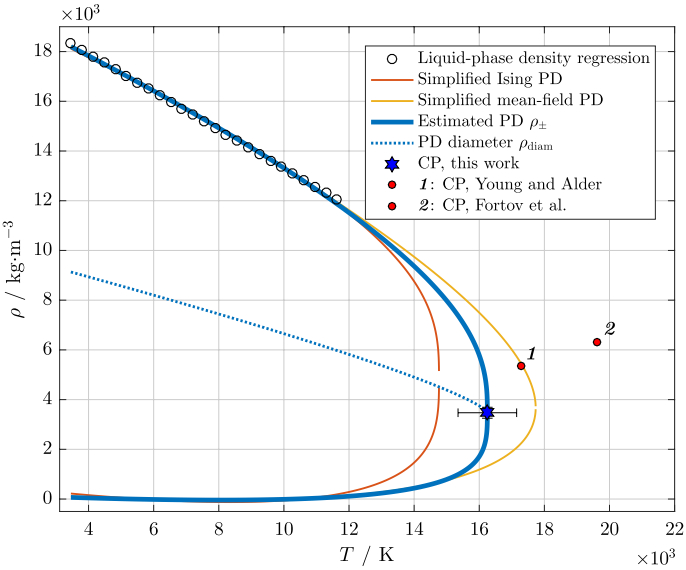

Fig. 4 Density ρ as a function of temperature T of rhenium up to the critical point (CP). Open circles represent data points generated from the density regression. Thin solid lines show the estimated phase diagram (PD) according to a simplified Ising and mean-field behavior. The best estimate for the phase diagram $\rho_{\pm}$ is indicated by a thick solid line, terminating in the critical point (star). The corresponding phase diagram diameter ρ_{diam} is plotted as dotted line. Critical points reported in the literature are indicated by red dots: Young and Alder [37], Fortov et al. [34]

$$T_{\mathrm{c}} = (16.3 \pm 0.9) \times 10^3\ \mathrm{K},$$
$$\rho_{\mathrm{c}} = (3.47 \pm 0.22) \times 10^3\ \mathrm{kg \cdot m^{-3}}\,.$$

The obtained critical density is the lowest among previously reported values. The value reported by Young and Alder applying the hard-sphere van der Waals model [37], $\rho_{\mathrm{c}} = 5.37 \times 10^3\ \mathrm{kg \cdot m^{-3}}$, is in satisfactory consistence with the simplified mean-field phase diagram, but it is considerably higher than this work's value. However, the reported critical temperature $T_{\mathrm{c}} = 17\,293\ \mathrm{K}$ is in good agreement with our value.

Fortov et al. report a critical density of $\rho_{\mathrm{c}} = 6.32 \times 10^3\ \mathrm{kg \cdot m^{-3}}$ and a critical temperature of $T_{\mathrm{c}} = 19\,600\ \mathrm{K}$ [34] (Grosse method). This extraordinary high critical temperature could only be reached, if our experimental data were extrapolated linearly up to this very high temperature. Therefore, the critical point stated by Fortov et al. appears to be incompatible with our estimation.

Further critical temperature values reported in the literature range from $T_{\mathrm{c}} = 12\,138\ \mathrm{K}$ (Hess and Schneidenbach [33], Guldberg rule) to $T_{\mathrm{c}} = (20\,660 \pm 540)\ \mathrm{K}$ (Lang [35], Kopp-Lang rule), where values reported earlier tend to be higher than more recent values. This is also the case for a critical temperature reported in 1961 by Grosse, $T_{\mathrm{c}} = 20\,500\ \mathrm{K}$ [38] (Grosse method). More recent

values given by Blairs and Abbasi [36] indicate that the critical temperature is lower than that: $T_c = 14\,608$ K (modified Gates-Thodos rule) and $T_c = 13\,398$ K (relation to surface tension).

For the critical pressure of rhenium, values of $p_c = 1.57$ GPa [34] and $p_c = 1.4877$ GPa [37] are stated in the literature.

5 Uncertainties

Uncertainties for experimental density values were estimated according to the GUM [39]. The so-obtained individual data point uncertainties in x- and y-direction were used to derive the GUM-conform uncertainties of regression intercept a and slope b according to [40]. These uncertainties were used together with the temperature uncertainty to calculate the density fit uncertainty at a given temperature, i.e., the temperature uncertainties were converted into density uncertainties via the slope of the regression. In the case of iridium, the relative combined expanded density uncertainty at a specific temperature (95 % confidence level, $k = 2$) increases from $U_c(\rho)/\rho = 0.012$ at melting to 0.049 at the highest temperature reached, for rhenium the uncertainty increases from $U_c(\rho)/\rho = 0.021$ to 0.065. For both elements, a room-temperature density standard uncertainty ($k = 1$) of $u(\rho_0) = 20\,\mathrm{kg \cdot m^{-3}}$ was assumed. For a more detailed general description, the reader is referred to [9, 12, 41].

The uncertainty of the critical point was estimated by executing the algorithm with slightly different density fit regressions, varied according to the coefficient uncertainties. Three cases were investigated, the normal density behavior with intercept a and slope b, the high and flat density behavior with $(a + u(a), b + u(b))$ and the low and steep density behavior $(a - u(a), b - u(b))$, where $b < 0$. The doubled standard deviation of the critical point observed in these three cases is reported as uncertainty. Note that this uncertainty is only a measure of how the critical point can change due to the uncertain fit coefficients of the linear density regression that is calculated from experimental data. However, this uncertainty can neither account for possibly inappropriate model functions used nor for approximative assumptions made in the estimation process, e.g., that results from different models may be averaged to yield a reasonable estimate for the investigated system. In a wider view, the uncertainty of the critical point may thus be extended out to the bounds given by the different models used. For the critical temperature, the resulting range is $\Delta T_{c,\mathrm{Ir}} = \pm 1.0 \times 10^3$ K and $\Delta T_{c,\mathrm{Re}} = \pm 1.5 \times 10^3$ K. For the critical density, this range ensues to $\Delta \rho_{c,\mathrm{Ir}} = \pm 0.81 \times 10^3\,\mathrm{kg \cdot m^{-3}}$ and $\Delta \rho_{c,\mathrm{Re}} = \pm 0.77 \times 10^3\,\mathrm{kg \cdot m^{-3}}$.

6 Conclusion

The density as a function of temperature was determined for liquid iridium and rhenium by means of ohmic pulse-heating. Experiments at 0.23 MPa were complemented by high-pressure experiments at up to 0.30 GPa to reach even higher temperatures. The experiments performed on iridium allowed to extend the accessible temperature range by more than 2000 K compared to data reported in the literature. For rhenium, the determined data reach more than 6000 K further into the liquid phase than previously reported literature data do. In both cases, the density as a function of temperature was shown to behave linearly up to the highest temperatures addressed. The experimental density data were used to estimate the critical density and critical temperature and to construct the full phase diagram making use of the Schröer–Pottlacher approach. Consistent with previous studies of our working group, this approach yields estimates for the critical temperature that are in the lower middle range of those reported in the literature and a critical density that resides at the low end of the reported values. The presence of higher critical densities in the literature may be partially explained by the frequent application of the rectilinear diameter rule. In general, the Schröer–Pottlacher algorithm yields satisfactory estimates but is strongly dependent on the temperature range of the input data. As long as no non-linearity in the density–temperature behavior is observed, i.e., as long as the input density shows a linear decrease with temperature, the algorithm provides a lower limit for the critical temperature, and an upper limit for the critical density.

Acknowledgements Open access funding provided by Graz University of Technology.

Compliance with Ethical Standards

Conflict of Interest The authors declare that they have no conflicts of interest.

References

1. T. Iida, R.I. Guthrie, *The Physical Properties of Liquid Metals* (Clarendon Press, Oxford, 1988)
2. P.F. Paradis, T. Ishikawa, R. Fujii, S. Yoda, Physical properties of liquid and undercooled tungsten by levitation techniques. Appl. Phys. Lett. **86**(4), 041901 (2005). https://doi.org/10.1063/1.1853513

3. D.M. Matson, X. Xiao, J.E. Rodriguez, J. Lee, R.W. Hyers, O. Shuleshova, I. Kaban, S. Schneider, C. Karrasch, S. Burggraff, R. Wunderlich, H.J. Fecht, Use of thermophysical properties to select and control convection during rapid solidification of steel alloys using electromagnetic levitation on the space station. JOM **69**(8), 1311 (2017). https://doi.org/10.1007/s11837-017-2396-5
4. P. Quested, R. Morrell, A. Dinsdale, L. Chapman, The measurement and estimation of density for selected liquid alloys. High Temp. High Press. **47**(4), 365 (2018)
5. A. Schmon, Density Determination of Liquid Metals by Means of Containerless Techniques. Doctoral thesis (2016)
6. A. Schmon, K. Aziz, G. Pottlacher, Density determination of liquid copper and liquid nickel by means of fast resistive pulse heating and electromagnetic levitation. Metall. Mater. Trans. A **46**(6), 2674 (2015). https://doi.org/10.1007/s11661-015-2844-1
7. A. Schmon, K. Aziz, M. Luckabauer, G. Pottlacher, Thermophysical properties of manganin (Cu86Mn12Ni2) in the solid and liquid state. Int. J. Thermophys. **36**(7), 1618 (2015). https://doi.org/10.1007/s10765-015-1909-0
8. M. Leitner, T. Leitner, A. Schmon, K. Aziz, G. Pottlacher, Thermophysical properties of liquid aluminum. Metall. Mater. Trans. A **48**(6), 3036 (2017). https://doi.org/10.1007/s11661-017-4053-6
9. M. Leitner, W. Schröer, G. Pottlacher, Density of liquid tantalum and estimation of critical point data. Int. J. Thermophys. **39**(11), 124 (2018). https://doi.org/10.1007/s10765-018-2439-3
10. M. Leitner, G. Pottlacher, Density of liquid niobium and tungsten and the estimation of critical point data. Metall. Mater. Trans. A **50**(8), 3646 (2019). https://doi.org/10.1007/s11661-019-05262-5
11. P. Pichler, B.J. Simonds, J.W. Sowards, G. Pottlacher, Measurements of thermophysical properties of solid and liquid NIST SRM 316L stainless steel. J. Mater. Sci. **55**(9), 4081 (2019). https://doi.org/10.1007/s10853-019-04261-6
12. M. Leitner, Density of Liquid High-Melting Metals and the Estimation of Critical Point Data. Doctoral thesis (2019)
13. G.R. Gathers, J.W. Shaner, W.M. Hodgson, Thermodynamic characterization of liquid metals at high temperature by isobaric expansion measurements. High Temp. High Press. **11**(5), 529 (1979)
14. S. Taioli, C. Cazorla, M.J. Gillan, D. Alfè, Melting curve of tantalum from first principles. Phys. Rev. B **75**(21), 214103 (2007). https://doi.org/10.1103/PhysRevB.75.214103
15. W. Schröer, G. Pottlacher, Estimation of critical data and phase diagrams of pure molten metals. High Temp. - High Press. **43**(2–3), 201 (2014)
16. G. Pottlacher, Bestimmung thermophysikalischer Daten von Metallen bis in den Überhitzungsbereich der flüssigen Phase. Doctoral thesis (1987)
17. Y. Marcus, On the compressibility of liquid metals. J. Chem. Thermodyn. **109**, 11 (2017). https://doi.org/10.1016/j.jct.2016.07.027
18. C. Cagran, G. Pottlacher, Thermophysical properties and normal spectral emittance of iridium up to 3500 K. Int. J. Thermophys. **28**(7), 697 (2007). https://doi.org/10.1007/s10765-007-0188-9
19. R. Bedford, G. Bonnier, H. Maas, F. Pavese, Recommended values of temperature on the International Temperature Scale of 1990 for a selected set of secondary reference points. Metrologia **33**(2), 133 (1996). https://doi.org/10.1088/0026-1394/33/2/3
20. J.W. Arblaster, Densities of osmium and iridium. Platinum Met. Rev. **33**(1), 14 (1989)
21. C. Cagran, B. Wilthan, G. Pottlacher, Normal spectral emissivities (at 684.5 nm) of liquid gold, rhenium, titanium and vanadium, conference proceedings Tempmeko. pp. 1313–1318 (2004)
22. W.M. Haynes (ed.), *CRC Handbook of Chemistry and Physics*, 96th edn. (Boca Raton, CRC Press, 2015– 2016)
23. D.R. Lide (ed.), *CRC Handbook of Chemistry and Physics*, 85th edn. (CRC Press, Boca Raton, 2004)
24. J.W. Shaner, G.R. Gathers, C. Minichino, Thermophysical properties of liquid tantalum and molybdenum. High Temp. High Press. **9**(3), 331 (1977)
25. T. Hüpf, Density Determination of Liquid Metals. Doctoral thesis (2010)
26. T. Ishikawa, C. Koyama, P.F. Paradis, J.T. Okada, Y. Nakata, Y. Watanabe, Densities of liquid Re, Os, and Ir, and their temperature dependence measured by an electrostatic levitator. Int. J. Refract. Met. Hard Mater. (2020). https://doi.org/10.1016/j.ijrmhm.2020.105305
27. T. Hüpf, G. Pottlacher, Thermal expansion of Ir, Pd, Pt, and V obtained in fast pulse-heating experiments. High Temp. High Press. **40**(3–4), 271 (2011)

28. G.R. Gathers, J.W. Shaner, R.S. Hixson, D.A. Young, Very high temperature thermophysical properties of solid and liquid vanadium and iridium. High Temp. High Press. **11**(6), 653 (1979)
29. P.F. Paradis, T. Ishikawa, S. Yoda, Noncontact density measurements of tantalum and rhenium in the liquid and undercooled states. Appl. Phys. Lett. **83**(19), 4047 (2003). https://doi.org/10.1063/1.1624475
30. T. Hüpf, C. Cagran, G. Lohöfer, G. Pottlacher, Electrical resistivity of high temperature metallic melts-Hf-3% Zr, Re, Fe Co, and Ni. High Temp. High Press. **37**(3), 239 (2008)
31. T. Thévenin, L. Arlès, M. Boivineau, J. Vermeulen, Thermophysical properties of Rhenium. Int. J. Thermophys. **14**(3), 441 (1993). https://doi.org/10.1007/BF00566043
32. R. Hixson, M. Winkler, Thermophysical properties of molybdenum and rhenium. Int. J. Thermophys. **13**(3), 477 (1992). https://doi.org/10.1007/bf00503884
33. H. Hess, H. Schneidenbach, On the estimation of critical point data of transition metals. Z. Metallkde. **87**(12), 979 (1996)
34. V.E. Fortov, A.N. Dremin, A.A. Leont'ev, Evaluation of the parameters of the critical point. Teplofiz. Vys. Temp. **13**(5), 1072 (1974)
35. G. Lang, Kritische Temperaturen und Temperaturkoeffizienten der Oberflächenspannung flüssiger Metalle. Z. Metallkde. **68**(3), 213 (1977)
36. S. Blairs, M.H. Abbasi, Correlation between surface tension and critical temperatures of liquid metals. J. Colloid Interface Sci. **304**(2), 549 (2006). https://doi.org/10.1016/j.jcis.2006.07.072
37. D.A. Young, B.J. Alder, Critical Point of Metals from the van der Waals Model. Phys. Rev. A **3**(1), 364 (1971). https://doi.org/10.1103/physreva.3.364
38. A. Grosse, The temperature range of liquid metals and an estimate of their critical constants. J. Inorg. Nucl. Chem. **22**(1–2), 23 (1961). https://doi.org/10.1016/0022-1902(61)80225-x
39. W.G.. of the Joint Committee for Guides in Metrology (JCGM/WG 1), *Evaluation of measurement data - Guide to the expression of uncertainty in measurement* (JCGM, 2008)
40. M. Matus, Koeffizienten und Ausgleichsrechnung: Die Messunsicherheit nach GUM, Teil 1: Ausgleichsgeraden. Tech. Mess. **72**(10), 584 (2005). https://doi.org/10.1524/teme.2005.72.10_2005.584
41. B. Wilthan, Verhalten des Emissionsgrades und thermophysikalische Daten von Legierungen bis in die flüssige Phase mit einer Unsicherheitsanalyse aller Messgrößen. Doctoral thesis (2005)